Critical behavior near the many-body localization transition in driven open systems

Zala Lenarčič[1],* Ori Alberton[2],* Achim Rosch[2], and Ehud Altman[1]
[1] *Department of Physics, University of California, Berkeley, California 94720, USA and*
[2] *Institute for Theoretical Physics, University of Cologne, D-50937 Cologne, Germany*

Coupling a many-body localized system to a thermal bath breaks local conservation laws and washes out signatures of localization. When the bath is non-thermal or when the system is also weakly driven, local conserved quantities acquire a highly non-thermal stationary value. We demonstrate how this property can be used to study the many-body localization phase transition in weakly open systems. Here, the strength of the coupling to the non-thermal baths plays a similar role as a finite temperature in a $T = 0$ quantum phase transition. By tuning this parameter, we can detect key features of the MBL transition: the divergence of the dynamical exponent due to Griffiths effects in one dimension and the critical disorder strength. We apply these ideas to study the MBL critical point numerically. The possibility to observe critical signatures of the MBL transition in an open system allows for new numerical approaches that overcome the limitations of exact diagonalization studies. Here we propose a scalable numerical scheme to study the MBL critical point using matrix-product operator solution to the Lindblad equation.

arXiv:1910.01548v2 [cond-mat.str-el] 13 Aug 2020

Many-body localization is a state of interacting quantum systems, which fail to thermalize subject to their intrinsic dynamics due to the effect of strong disorder [1–3]. A pertinent question, currently under intense theoretical study and debate, concerns the nature of the phase transition between the ergodic and localized phases. The transition represents a new class of dynamical quantum phase transitions, which involves a fundamental change of the entanglement structure in all, or at least many, of the eigenstates. The many-body localization transition is sharp only if the system is completely isolated, which imposes severe limitations on the ability to study it using standard theoretical, numerical, and experimental approaches. The requirement of a closed system appears to preclude experiments with solid state materials due to coupling to a phonon bath. Even in experiments with ultra-cold atoms and ion traps, which are usually considered to be exquisitely isolated, signatures of many-body localization are visibly polluted by extrinsic decay processes [4–7]. Numerical experiments are also severely limited. Because of the need to address closed system dynamics, these have been mostly restricted to exact diagonalization (ED) of very small systems [8–14]. There is increasing evidence that such simulations are overwhelmed by transient finite-size effects that supersede the critical scaling behavior[15–17].

We propose to bypass the limitations posed by closed systems by studying signatures of the MBL transition in weakly open driven systems. In a previous work [18] some of us showed that in the limit of vanishing coupling ϵ to a bath and concomitantly weak drive strength $\epsilon\theta$, the MBL transition shows up as a singular change in the temperature variations across the sample. On the thermalizing side of the critical point the temperature fluctuations vanish in the limit $\epsilon \to 0$, while they remain finite on the MBL side. At non-vanishing coupling ϵ one expects this transition to broaden into a universal crossover governed by the critical point located at $\epsilon \to 0$. The dissipative coupling ϵ has a role similar to turning on a nonzero temperature above a $T = 0$ quantum phase transition. Studying the leading dependence of the spatial temperature fluctuations on ϵ in the vicinity of the critical point is analogous to studying the leading dependence of the order parameter on the temperature in a conventional quantum phase transition. Such a measurement allows to determine critical exponents as well as the critical disorder strength. Furthermore, the MBL transition in one dimensional systems is thought to be preceded by a thermal Griffiths regime leading to subdiffusive transport [19–38]. We use an effective model of the Griffiths phase to show that the leading dependence of the temperature variations on the dissipative coupling ϵ reveals the continuously varying dynamical exponent z.

The open systems framework facilitates a new computational scheme to investigate the MBL transition, while overcoming the limitations of exact diagonalization. We use a truncated matrix-product operator to represent the density matrix of a disordered system described by a Lindblad equation with coupling ϵ to dissipators. We find a sharp signature of the Griffith regime with a continuously varying dynamical exponent that diverges at the critical point. We note the connection to Refs. [24, 35, 38], where Griffiths exponents have been computed numerically for a spin-chain coupled to Lindblad operators placed at the two ends of the chain to drive a steady state current. Because we study coupling to bulk Lindblad operators, the calculation can converge faster, allowing to access parameter regimes much closer to the MBL transition.

Hydrodynamic description– Consider a disordered ergodic system, weakly coupled to a thermal bath with temperature T_0 and a drive that heats the system; for example, a spin chain, coupled to phonons and driven by light [18]. Deep in the ergodic phase the system will reach a nearly thermal steady state, with smooth temperature variations determined by a heat flow equation

* These two authors contributed equally

supplemented by sink and source terms due to the coupling to the bath and drive, respectively,

$$\partial_t e(\boldsymbol{r}) - \nabla\cdot(\kappa(\boldsymbol{r})\nabla T(\boldsymbol{r})) = -\epsilon\, g_1(\boldsymbol{r})(T(\boldsymbol{r})-T_0) + \epsilon\,\theta g_2(\boldsymbol{r}) \tag{1}$$

We assumed, for simplicity, that energy is the only conserved quantity in the limit $\epsilon \to 0$. The disorder in the underlying model is translated to a weak modulation of the conductivity $\kappa(\boldsymbol{r}) = \bar{\kappa} + \delta\kappa(\boldsymbol{r})$ and of the couplings $g_{1(2)}(\boldsymbol{r}) = \bar{g} + \delta g_{1(2)}(\boldsymbol{r})$ to the thermal bath ($g_1(\boldsymbol{r})$) and the drive ($\theta g_2(\boldsymbol{r})$). The temperature profile varies around the mean value, $T(\boldsymbol{r}) = \bar{T} + \delta T(\boldsymbol{r})$, where the mean temperature $\bar{T} = T_0 + \theta$ is determined by the relative strength θ of the drive compared to the coupling to the bath.

Linearizing Eq. (27) in the disorder strength for the steady state gives $(-\bar{\kappa}\nabla^2 + \epsilon\bar{g})\delta T(\boldsymbol{r}) = \epsilon\,\theta\,\delta g(\boldsymbol{r})$, where $\delta g(\boldsymbol{r}) = \delta g_2(\boldsymbol{r}) - \delta g_1(\boldsymbol{r})$. This equation is solved for the local temperature variations using the Green's function, $\delta T(\boldsymbol{r}) = \epsilon\theta \int d\boldsymbol{r}' G(\boldsymbol{r}-\boldsymbol{r}')\delta g(\boldsymbol{r}')$, which is in momentum space given by $\tilde{G}(\boldsymbol{k}) = \left(\bar{\kappa}\,k^2 + \bar{g}\,\epsilon\right)^{-1}$. We can generalize to the sub-diffusive regime heuristically by using a renormalized Green's function, $G(\boldsymbol{k}) = (\bar{\gamma}|k|^z + \bar{g}\,\epsilon)^{-1}$, imposing dynamical scaling with exponent $z \geq 2$. Assuming Gaussian disorder with short range correlations, $\langle \delta g(\boldsymbol{r})\delta g(\boldsymbol{r}')\rangle \equiv (\delta g)^2\delta(\boldsymbol{r}-\boldsymbol{r}')$, we find in d dimensions,

$$\delta T \sim \theta\,|\delta g/\bar{g}|\,(\bar{g}/\bar{\gamma})^{d/2z}\;\epsilon^{d/2z}, \tag{2}$$

see Suppl. Mat. (SM), [39]. This approach, however, may not properly account for the effect of rare regions that dominate the transport in the Griffiths regime. Below we examine a minimal model that takes this physics into account.

Thermal resistor network – As a minimal model for the Griffiths regime we consider a chain of conducting islands, each characterized by its own temperature T_i, coupled by links representing insulating regions of size ℓ. Together with the energy sink and source terms, this leads to rate equations

$$\begin{aligned}\partial_t e_i - \Gamma_{i,i+1}(T_{i+1}-T_i) + \Gamma_{i-1,i}(T_i - T_{i-1}) \\ = -\epsilon g_{1,i}(T_i - T_0) + \epsilon\theta g_{2,i}.\end{aligned} \tag{3}$$

While this equation may look like a simple discretization of Eq. (27), there is a crucial difference coming from the probability distribution of the link conductances. An 'insulating' link of length ℓ has conductance $\Gamma_{\rm ins}(\ell) = \Gamma_0 e^{-\ell/a}$ with a being a microscopic scale. Close to the critical point we expect the lengths distribution of insulating regions to be $p(\ell) = \frac{1}{\mathcal{N}} e^{-\ell/\xi}$ with ξ the diverging correlation length, leading to the distribution of link conductances $P(\Gamma) \sim (\Gamma/\Gamma_0)^{\alpha-1}$ with $\alpha = a/\xi \ll 1$. In this case the average resistivity of the chain $\langle \Gamma^{-1}\rangle$ diverges, indicating sub-diffusive transport [21, 40].

Coupling this system to a bath and to an energy source destroys the insulating behavior of the links, adding a channel of conductance through the link with conductivity $\epsilon\kappa_0$. Thus we take the heat conductance through a link to be $\Gamma = \epsilon\frac{\kappa_0}{\ell} + \Gamma_0 e^{-\ell/a}$, with an implicit cutoff $\ell \geq a$. Finally we take $g_{1(2),i} = \bar{g} + \delta g_{1(2),i}$ with $\delta g_{1(2),i}$ drawn from a uniform distribution in the range $[-\delta g_{1(2)}, \delta g_{1(2)}]$.

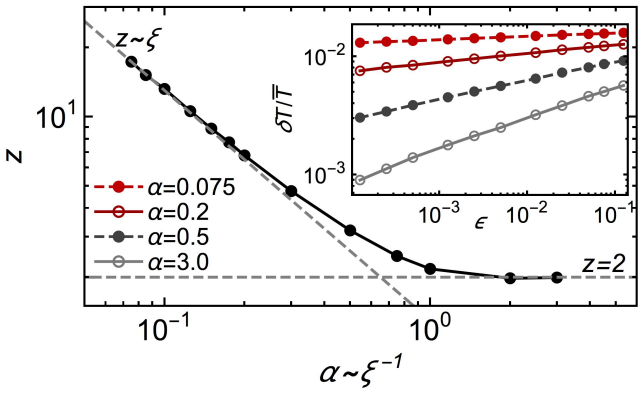


FIG. 1. Fluctuations of the local temperatures, $\delta T/\bar{T}$, are computed from a resistor network model as function of the coupling strength ϵ to a thermal bath and driving. For small ϵ, temperature fluctuations are described by $\delta T/\bar{T} \sim \epsilon^{1/2z}$ with $z \sim \alpha^{-1} = \xi/a$ for $0 < \alpha < 1$, and $z = 2$ in the diffusive regime, $\alpha > 1$. Parameters: $\kappa_0 = 1$, $a\Gamma_0 = 5.0$, $T_0 = 1$, $\delta g_1 = 0.05$, $\delta g_2 = 0.05$, $\theta = T_0$, $N = 1000$, averaged over $M = 500$ configurations.

We solve for the steady state of Eq. (3) numerically to obtain temperature profiles and extract the normalized variation of local temperatures $\delta T/\bar{T} = \sqrt{\langle\langle \mathrm{Var}(T_i)\rangle\rangle}/\langle\langle \mathbb{E}(T_i)\rangle\rangle$. Here $\mathbb{E}$ and Var are the sample mean and variance, while $\langle\langle\cdot\rangle\rangle$ denotes averaging over disorder realizations. We assumed that the conducting islands are all of similar size.

The results for $\delta T/\bar{T}$ as a function of ϵ are shown in Fig. 1 for different values of $\alpha = a/\xi$. We get $\delta T \sim \epsilon^{1/2z}$ as anticipated in Eq. (2). We see that for $0 < \alpha < 1$ the dynamical exponent grows with the correlation length as $z \sim 1/\alpha = \xi/a$, whereas for $\alpha > 1$ it saturates to $z = 2$, as expected for a diffusive system. Thus we establish a direct relation between the leading dependence of the temperature fluctuations δT on ϵ and the dynamical exponent z, which governs the sub-diffusive behavior in a closed system [41, 42].

Before proceeding we comment on the behavior of the thermal resistor network in two dimensions. It is shown in the SM that in this case we have $\delta T \sim \epsilon^{d/4}$, implying $z = 2$ for all α. This is also the expected dynamical behavior in a two dimensional closed system because any rare region with large resistance can be short circuited by surrounding smaller resistors [43].

Charge transport – In solid state systems it is usually much easier to measure charge transport than the local temperature profile. It is therefore natural to seek signatures of MBL or the Griffiths regimes in the resistance of a weakly open system. In order to compute how the

resistance scales with the external bath or drive coupling ϵ we consider a charge resistor network described by

$$\partial_t n_i - \left(\tilde{\Gamma}_{i,i+1}(\mu_{i+1}-\mu_i) - \tilde{\Gamma}_{i-1,i}(\mu_i-\mu_{i-1})\right) = 0. \quad (4)$$

Here μ_i is the electro-chemical potential on island i. $\tilde{\Gamma}_{i,j}$ are charge conductances on links, which are distributed exactly as the thermal conductances in Eq. (3). Unlike in Eq. (3), there are no source or sink terms because the external coupling to the bath and the drive are assumed to conserve charge. In fact, we can consider a system with just a drive or just tunable coupling to phonons. Both give rise to a parallel channel of ohmic conductivity proportional to ϵ on the insulating links, $\tilde{\Gamma}(\ell) = \tilde{\Gamma}_0 e^{-\ell/a} + \epsilon\sigma_0/\ell$. Comparing the first and second term we see that the insulating behavior dominates for $\ell < \ell_* \approx a\ln\epsilon^{-1} + a\ln\ln\epsilon^{-1}$, while the bath or drive induced conductance dominates in longer links. To gain analytic insight we calculate the average resistivity of the chain, $\bar{\rho} = \bar{\ell}^{-1}\int d\ell P(\ell)\tilde{\Gamma}(\ell)^{-1}$,

$$\bar{\rho} \approx \frac{1}{\bar{\ell}\tilde{\Gamma}_0}\int_a^{\ell_*} d\ell\xi^{-1}e^{\ell(a^{-1}-\xi^{-1})} \approx \frac{\alpha}{\bar{\ell}\tilde{\Gamma}_0}\left(\frac{\epsilon}{\ln\epsilon^{-1}}\right)^{\alpha-1} \quad (5)$$

where $\alpha = a/\xi \sim 1/z$ and $\bar{\ell} = \int \mathrm{d}\ell P(\ell)\ell \sim \xi$. A numerical solution confirms this result, see SM. Thus it should be possible to measure the dynamical exponent z by varying the coupling ϵ via controlled cooling of the phonon bath or by varying the strength of an external drive.

Numerical solution of a spin model – Consideration of weakly open driven systems suggests a new approach for investigating the MBL transition numerically. Here we calculate how the local temperature variations in a spin-chain model change with the coupling to a weak drive that brings the system to a non-thermal steady state. The coherent part of the dynamics is governed by the Hamiltonian

$$H = \sum_i S_i \cdot S_{i+1} + h(\zeta_i^z S_i^z + \zeta_i^x S_i^x) \quad (6)$$

with open boundary conditions and disorder fields drawn uniformly from the range $\zeta_i^{x,z} \in [-1,1]$. For simplicity we have chosen a model in which energy is the only conserved quantity. The MBL transition in the Hamiltonian (6) has been studied in Ref. [44] using exact diagonalization.

To obtain a non-equilibrium steady state we model weak coupling of the system to non-thermal baths within a Lindblad formalism:

$$\dot{\rho} = -i[H,\rho] + \epsilon\sum_{\nu,i}\left(L_i^\nu \rho L_i^{\nu\dagger} - \frac{1}{2}\{L_i^{\nu\dagger}L_i^\nu,\rho\}\right). \quad (7)$$

with the Lindblad operators

$$L_i^{\pm,1} = \frac{S_i^\pm}{2\sqrt{2}}\left(\mathbb{1} - 2S_{i+1}^z\right),\ L_i^{\pm,2} = \left(\mathbb{1} - 2S_i^z\right)\frac{S_{i+1}^\pm}{2\sqrt{2}},$$
$$L_i^z = S_i^z. \quad (8)$$

The precise choice is not important as long as some of the dissipators are non-Hermitian to ensure a non-trivial steady state, $\rho_\infty \neq \mathbb{1}$. In particular, we show in the SM. that a generic Lindblad equation leads to the hydrodynamic Eq. (27) for the smooth temperature variations.

The (unique) steady state ρ_∞ is obtained by solving the Lindblad time evolution using the time-evolving block decimation (TEBD) technique for a vectorized density matrix [45, 46]. The dephasing term L_i^z, Eq. (8), is used to ensure that the steady state is sufficiently close to the identity, so that a bond dimension of $\chi = 100$ is adequate to describe a system of $N = 20$ sites for $\epsilon \geq 0.01$. A larger bond dimensions and longer propagation times are needed for smaller ϵ, making computation in these cases more expensive, see SM. At fixed h, the same set of disorder configurations is used for different values of ϵ, while independent configurations are used at different values of h. This procedure helps to determine the exponent z as the ϵ dependence becomes less affected by the statistical ensemble. We average over 100 ($h = 1, 2$) or 300-500 ($h > 2$) disorder configurations.

The goal of the calculation is to obtain the spatial variation of the local temperature for varying values of the dissipative coupling ϵ. To determine the local temperatures T_i we compare the two-site reduced density matrix of the steady state $\rho_\infty^{(i,i+1)}$ with a thermal state [47] by minimizing $F[T_i] = \mathrm{Tr}\left[\left(\rho_\infty^{(i,i+1)} - \rho_{\mathrm{th}}^{(i,i+1)}(T_i)\right)^2\right]$ with respect to T_i. We chose two sites as the minimal cluster that contains the non-local couplings in the Lindblad equation.

The inverse temperature variations $\delta\beta/\bar{\beta}$, obtained numerically as a function of ϵ, are shown in Fig. 2 for a range of disorder strengths. We observe different ϵ dependence in the MBL and ergodic phase, namely

$$\frac{\delta\beta}{\bar{\beta}}(\epsilon) \sim \begin{cases} \epsilon^{1/2z}, & h < h_c, \\ \frac{\delta\beta}{\bar{\beta}}\big|_{\epsilon\to 0} - b\,\epsilon + \mathcal{O}(\epsilon^2), & h \geq h_c \end{cases}. \quad (9)$$

In the MBL phase we see temperature variations of order one even in the limit $\epsilon \to 0$ as predicted in Ref. [18]. At finite ϵ we expect an analytic dependence on ϵ due to the local nature of the MBL phase. In the thermal regime, the temperature variations are expected to vanish in the limit $\epsilon \to 0$ [18]. We see an increase of the temperature variations with ϵ that fits well with the expected non-analytic behavior $\delta\beta/\bar{\beta} \sim \epsilon^{1/2z}$ at small values of ϵ, see Fig. 2(b). The fitted dynamical exponent z, shown in Fig. 3, changes continuously with disorder strength, growing rapidly as the MBL transition is approached. Error bars in Fig. 2c and Fig. 3 were obtained using bootstrap and jackknife resampling, respectively. The usage of a resampling methods for error estimates is necessary because statistical errors for different ϵ at fixed h are strongly correlated in our setup. As discussed above, the dynamical exponent is expected to diverge together with the correlation length ξ at the MBL critical point. The apparent saturation of z is an artifact of the fit procedure and not a finite-size effect; it is impossible to fit a small γ to the function ϵ^γ for realistic values of $\epsilon \gtrsim 0.01$. Thus the minimal value of ϵ limits the ac-

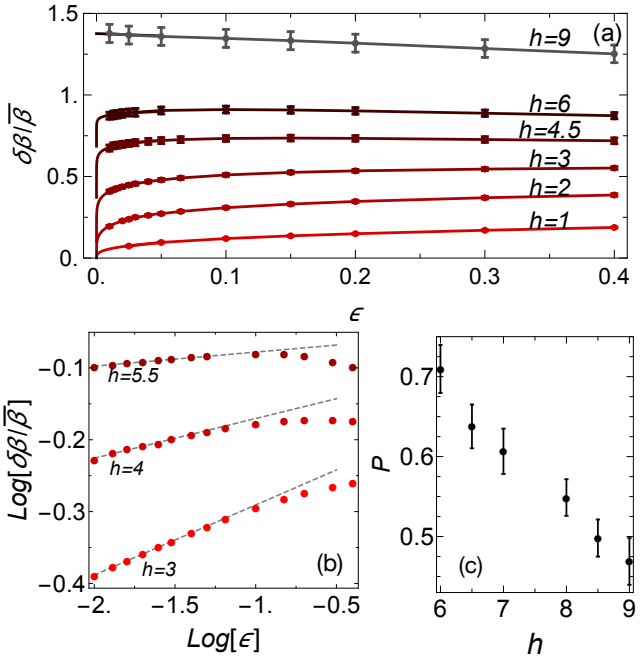


FIG. 2. *Numerical Time Evolving Block Decimation results* – (a) The fluctuations of the inverse temperature, $\delta\beta/\bar{\beta}$, show two distinct dependences on ϵ: while they vanish proportionally to $\epsilon^{1/2z}$ on the ergodic side of the phase diagram, they obtain a finite value for $\epsilon \to 0$ with a linear correction in the MBL phase. Errorbars show (a correlated) statistical error, while line correspond to the fits. (b) Fits (dashed lines) to $\delta\beta/\bar{\beta}$ are used to obtain $z(h)$ shown in Fig. 3. (c) We estimate $h_c \approx 8.75 \pm 0.5$ from the condition that at h_c the probability P for $\delta\beta/\bar{\beta}$ to have a positive slope at smallest ϵ equals $P = 0.5$. That is, at h_c the sign of the slope is undetermined.

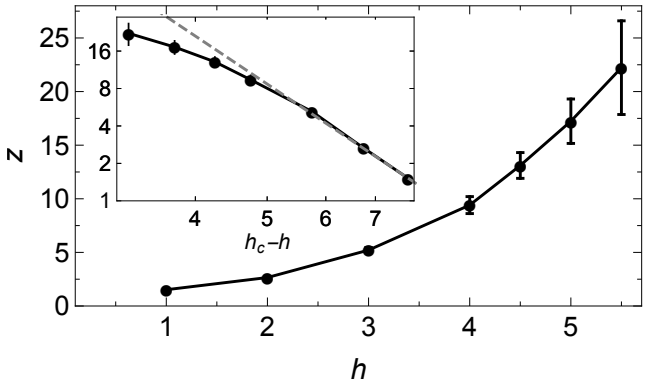


FIG. 3. The dynamical exponent z increases sharply upon approaching the MBL phase transition. The apparent saturation is due to limitation to $\epsilon \geq 0.01$. Inset: z as function of $h_c - h$ on log-log scale assuming $h_c = 8.75$. Using $h_c = 8.75 \pm 0.5$, our results are consistent with $z \sim (h - h_c)^{-\nu}$ with critical exponent $\nu = 4 \pm 0.9$ (dashed line).

curacy by which we can determine the critical disorder strength and the critical exponents. See SM for a systematic finite-size analysis and other numerical aspects.

We obtain a lower bound on the critical disorder strength h_c by recording the fraction P of disorder realizations showing $\delta\beta/\bar{\beta}$ increasing with ϵ near $\epsilon = 0.01$, Fig. 2(c). The estimation of h_c is also limited by the minimal $\epsilon = 0.01$ as h_c may increase somewhat if we use a smaller ϵ. From condition $P = 0.5$ we estimate $h_c \geq 8.75 \pm 0.5$ for $N = 20$, higher than the value $2 < h_c < 7$ estimated from an ED study of the same model [44]. This is consistent with recent analyses suggesting that ED results significantly underestimate h_c due to slow convergence of level spacing statistics [15–17]. Broadening of levels by the dissipative coupling appears to resolve these issues.

We extract a correlation length exponent ν from the divergence of $z \sim \xi \sim (h_c - h)^{-\nu}$. Using $h_c = 8.75 \pm 0.5$, we estimate $\nu \approx 4.0 \pm 0.9$, which is consistent with the Harris-Chayes bound, $\nu > 2/d$ [48, 49] and in agreement with single parameter scaling fits to renormalization group results [41, 42]. But we caution that when using $\epsilon \geq 0.01$ we can reliably fit an exponent only in the range $h \in [1, 4]$, not very close to the critical disorder strength. Based on our current data we cannot exclude Kosterlitz-Thouless like scaling with $z \sim \xi \sim e^{c/\sqrt{h_c - h}}$ as suggested by recent works [50, 51].

It is an interesting question how the "order parameter" $\delta\beta/\bar{\beta}$ behaves at the critical point itself $h = h_c$ in the limit $\epsilon \to 0$. Our results are consistent with a jump across the transition, but they also leave open the possibility of a logarithmic behavior as $-1/\log\epsilon$, which would allow a continuous change of $\delta\beta/\bar{\beta}$ across the transition.

Discussion – We have demonstrated the advantages of investigating the MBL transition as a function of the coupling strength ϵ to external non-equilibrium baths. In numerical computations, the finite coupling to baths limits the operator entanglement entropy allowing to use powerful matrix-product operator methods on both sides of the phase transition. We were able to obtain quantitative information on quantum critical properties, including the dynamical exponent z, the correlation length exponent ν and the critical disorder strength h_c. Moreover, having a weak coupling to the baths seems to regulate the calculation by broadening the many-body energy levels facilitating faster convergence to the asymptotic scaling limit. We also obtain a lower bound on h_c, which is much larger than h_c found by direct analysis of ED results [44]. This is consistent with recent analyses [15–17], which suggests that h_c is significantly underestimated by ED studies.

Our numerical scheme is scalable in terms of the calculated spatial size. The limiting factor, instead, is the timescale imposed by the minimal value of the dissipative coupling ϵ. For the system size to dominate the critical scaling, the time $1/\epsilon$ would have to grow at least exponentially with L. This is a fundamental limitation stemming from the exponential dynamical scaling that characterizes the critical point.

Our approach to extract MBL from steady-state measurements in driven open systems is complementary to approaches studying the dynamics after a quench [4, 52] and opens the door to more experiments with solids in spite of the coupling to phonons. The non-equilibrium conditions discussed in the main text can be achieved by driving the system externally either with light, or with a bias voltage. Coupling strength to the environment would be tuned, e.g., by modulating the phonon temperature and the power of the light source. Local temperatures variations can be measured, for example by comparing the Stokes and Antistokes response in a local (tip-enhanced) Raman spectroscopy experiment [53, 54]. Another possibility would be a simpler resistivity measurement, where the dependence of the resistivity on the strength of coupling to phonons can also provide crucial information on the MBL transition.

ACKNOWLEDGMENTS

Our TEBD code was written in Julia [55], relying on the TensorOperations.jl package. We acknowledge useful discussions with V. Bulchandani, Y. Werman, M. Žnidarič. We acknowledge in part funding from Gordon and Betty Moore Foundation's EPIC initiative, Grant GBMF4545 and from the European Research Council (ERC) synergy UQUAM project (EA,ZL), from the ERC under the Horizon 2020 research and innovation program, Grant Agreement No. 647434 (DOQS) (OA), and from the German Science Foundation under CRC 1238 (project C04) (AR). We furthermore thank the Regional Computing Center of the University of Cologne (RRZK) for providing computing time on the DFG-funded High Performance Computing (HPC) system CHEOPS as well as support.

[1] D. Basko, I. Aleiner and B. Altshuler, Annals of Physics **321**, 1126 (2006).
[2] I. V. Gornyi, A. D. Mirlin and D. G. Polyakov, Phys. Rev. Lett. **95**, 206603 (2005).
[3] D. A. Abanin, E. Altman, I. Bloch and M. Serbyn, Rev. Mod. Phys. **91**, 021001 (2019).
[4] M. Schreiber *et al.*, Science **349**, 842 (2015).
[5] H. P. Lüschen, P. Bordia, S. Scherg, F. Alet, E. Altman, U. Schneider, and I. Bloch, Phys. Rev. Lett. **119**, 260401 (2017).
[6] A. Lukin *et al.*, Science **364**, 256 (2019).
[7] J. Smith *et al.*, Nat. Phys. **12**, 907 (2016).
[8] D. J. Luitz, N. Laflorencie and F. Alet, Phys. Rev. B **91**, 081103(R) (2015).
[9] V. Oganesyan and D. A. Huse, Phys. Rev. B **75**, 155111 (2007).
[10] A. Pal and D. A. Huse, Phys. Rev. B **82**, 174411 (2010).
[11] J. A. Kjäll, J. H. Bardarson and F. Pollmann, Phys. Rev. Lett. **113**, 107204 (2014).
[12] V. Khemani, S. P. Lim, D. N. Sheng and D. A. Huse, Phys. Rev. X **7**, 021013 (2017).
[13] M. Serbyn and J. E. Moore, Phys. Rev. B **93**, 041424(R) (2016).
[14] R. Vasseur, S. A. Parameswaran and J. E. Moore, Phys. Rev. B **91**, 140202(R) (2015).
[15] J. Šuntajs, J. Bonča, T. Prosen and L. Vidmar, arXiv:1905.06345 (2019).
[16] D. A. Abanin et al, arXiv:1911.04501 (2019).
[17] R. .K. Panda, A. Scardicchio, M. Schulz, S. R. Taylor, and M. Žnidarič, EPL 128 (2019) 67003.
[18] Z. Lenarčič, E. Altman and A. Rosch, Phys. Rev. Lett. **121**, 267603 (2018).
[19] M. Žnidarič, New Journal of Physics **12**, 043001 (2010).
[20] R. Nandkishore, S. Gopalakrishnan and D. A. Huse, Phys. Rev. B **90**, 064203 (2014).
[21] K. Agarwal, S. Gopalakrishnan, M. Knap, M. Müller and E. Demler, Phys. Rev. Lett. **114**, 160401 (2015).
[22] S. Johri, R. Nandkishore and R. N. Bhatt, Phys. Rev. Lett. **114**, 117401 (2015).
[23] M. H. Fischer, M. Maksymenko and E. Altman, Phys. Rev. Lett. **116**, 160401 (2016).
[24] M. Žnidarič, A. Scardicchio and V. K. Varma, Phys. Rev. Lett. **117**, 040601 (2016).
[25] M. V. Medvedyeva, T. Prosen and M. Žnidarič, Phys. Rev. B **93**, 094205 (2016).
[26] P. Bordia, H. P. Luschen, S. S. Hodgman, M. Schreiber, I. Bloch,U. Schneider, Phys. Rev. Lett. **116**, 140401 (2016).
[27] P. Prelovšek, Phys. Rev. B **94**, 144204 (2016).
[28] E. Levi, M. Heyl, I. Lesanovsky and J. P. Garrahan, Phys. Rev. Lett. **116**, 237203 (2016).
[29] H. P. Lüschen *et al.*, Phys. Rev. X **7**, 011034 (2017).
[30] D. J. Luitz, F. Huveneers and W. De Roeck, Phys. Rev. Lett. **119**, 150602 (2017).
[31] R. Nandkishore and S. Gopalakrishnan, Annalen der Physik **529** (2017).
[32] B. Everest, I. Lesanovsky, J. P. Garrahan and E. Levi, Phys. Rev. B **95**, 024310 (2017).
[33] J. Marino and R. M. Nandkishore, Phys. Rev. B **97**, 054201 (2018).
[34] A. Rubio-Abadal *et al.*, Phys. Rev. X 9, 041014 (2019).
[35] M. Schulz, S. R. Taylor, C. A. Hooley and A. Scardicchio, Phys. Rev. B **98**, 180201(R) (2018).
[36] F. Weiner, F. Evers and S. Bera, Phys. Rev. B **100**, 104204 (2019).
[37] M. Schulz, S. Taylor, A. Scardicchio and M. Žnidarič, J. Stat. Mech. (2020) 023107.
[38] J. J. Mendoza-Arenas, M. Žnidaric, V. K. Varma, J. Goold, S. R. Clark, A. Scardicchio, Phys. Rev. B **99**,

094435 (2019).
[39] See Supplementary Material for (i) a derivation of relation between temperature fluctuations and transport properties of disordered systems, (ii) a comparison to a more standard measure of subdiffusivity, (iii) resistor network results in two dimensions, (iv) the discussion on an alternative experimental realization involving current measurement, (v) numerical aspects of our TEBD calculation, (vi) a derivation on how the phenomenological terms in hydrodynamic description can emerge from the microscopic Liouville equation. Supplementary Material includes Refs. [18, 43, 56, 57].
[40] J. Hulin, J. Bouchaud and A. Georges, Journal of Physics A: Mathematical and General **23**, 1085 (1990).
[41] R. Vosk, D. A. Huse and E. Altman, Phys. Rev. X **5**, 031032 (2015).
[42] A. C. Potter, R. Vasseur and S. A. Parameswaran, Phys. Rev. X **5**, 031033 (2015).
[43] S. Gopalakrishnan, K. Agarwal, E. A. Demler, D. A. Huse and M. Knap, Phys. Rev. B **93**, 134206 (2016).
[44] S. D. Geraedts, N. Regnault and R. M. Nandkishore, New Journal of Physics **19**, 113021 (2017).
[45] F. Verstraete, J. J. García-Ripoll and J. I. Cirac, Phys. Rev. Lett. **93**, 207204 (2004).
[46] M. Zwolak and G. Vidal, Phys. Rev. Lett. **93** 207205, (2004).
[47] M. C. Bañuls, J. I. Cirac and M. B. Hastings, Phys. Rev. Lett. **106**, 050405 (2011).
[48] A. B. Harris, Journal of Physics C: Solid State Physics **7**, 3082 (1974).
[49] J. T. Chayes, L. Chayes, D. S. Fisher and T. Spencer, Phys. Rev. Lett. **57**, 2999 (1986).
[50] A. Goremykina, R. Vasseur and M. Serbyn, Phys. Rev. Lett. **122**, 040601 (2019).
[51] P. T. Dumitrescu, A. Goremykina, S. A. Parameswaran, M. Serbyn and R. Vasseur, Phys. Rev. B **99**, 094205 (2019).
[52] K. X. Wei, C. Ramanathan and P. Cappellaro, Phys. Rev. Lett. **120**, 070501 (2018).
[53] M. S. Anderson, Applied Physics Letters **76**, 3130 (2000).
[54] A. Sternbach *et al.*, arXiv:1706.08478 (2017).
[55] J. Bezanson, A. Edelman, S. Karpinski and V. B. Shah, SIAM review **59**, 65 (2017).
[56] S. Ş. Bayın, Journal of Mathematical Physics **57**, 123501 (2016).
[57] A. A. A. Kilbas, H. M. Srivastava and J. J. Trujillo, *Theory and applications of fractional differential equations* Vol. 204 (Elsevier Science Limited, 2006).

SUPPLEMENTARY MATERIAL

Fractional diffusion

In this section, we use the formalism of fractional calculus [56, 57] in order to generalize the hydrodynamic Eq. (1) to describe the sub- and super-diffusive case. The key idea is to modify the Greens function $G(\boldsymbol{r})$, describing the response of temperature fluctuations to a random pump and drive $\delta g(\boldsymbol{r})$ (recall that $\delta T(\boldsymbol{r}) = \epsilon\theta \int d\boldsymbol{r}' G(\boldsymbol{r}-\boldsymbol{r}')\delta g(\boldsymbol{r}')$), by replacing the Laplace operator ∇^2 with the Riesz fractional derivative ∇^z. The fractional derivative is defined via its Fourier transform $\mathcal{F}$,

$$\mathcal{F}\left(\boldsymbol{\nabla}^z y(\boldsymbol{r})\right) = -|k|^z \mathcal{F}(y(\boldsymbol{r})),\ z>0, \tag{10}$$

where $y(\boldsymbol{r})$ is an inifnitely differentiable function. Hence, the generalized continuity equation gives rise to the following Greens function in momentum space

$$G(\boldsymbol{k}) = \frac{1}{\bar{\gamma}|k|^z + \bar{g}\epsilon}. \tag{11}$$

Uncorrelated disorder $\langle \delta g(\boldsymbol{r})\delta g(\boldsymbol{r}')\rangle = (\delta g)^2\delta(\boldsymbol{r}-\boldsymbol{r}')$ gives the following scaling of temperature fluctuations with the dimension d and fractional power z

$$\begin{aligned}\langle \delta T^2\rangle &= \frac{\epsilon^2\theta^2}{L}\int G(\boldsymbol{r}-\boldsymbol{r}')G(\boldsymbol{r}-\boldsymbol{r}'')\langle \delta g(\boldsymbol{r}')\delta g(\boldsymbol{r}'')\rangle d\boldsymbol{r}d\boldsymbol{r}'d\boldsymbol{r}'' \\ &= \frac{\epsilon^2\theta^2\delta g^2}{(2\pi)^d}\int d\boldsymbol{k}\frac{1}{(\bar{\gamma}|k|^z+\epsilon\bar{g})^2} \\ &\sim \frac{\theta^2\delta g^2}{\bar{g}^2}\frac{\bar{g}^{d/z}}{\bar{\gamma}^{d/z}}\frac{(z-d)}{z^2\sin(d\pi/z)}\epsilon^{d/z},\end{aligned} \tag{12}$$

which is the result quoted in Eq. (2).

Diffusive behavior in two dimensions

In this section we generalize the random resistor model, used to describe the sub-diffusive behavior in the Griffiths regime of one dimensional systems, to the case of a two dimensional system. We will show how diffusive behavior emerges in this model throughout the thermal phase as long as the correlation length associated with the transition remains finite.

Our two dimensional toy model consists of a square lattice of conducting islands connected by insulating links of linear length ℓ taken from a probability distribution $p(\ell) \sim e^{-(\ell/\xi)^2}$ (and generally in d dimensions $p(\ell) \sim e^{-(\ell/\xi)^d}$). This takes into account that in higher dimensions insulating regions are harder to construct than in one dimension because they can be short circuited by conducting paths. Conductances across the links are given by

$$\Gamma = \epsilon\frac{\kappa_0}{\ell^{2-d}} + \Gamma_0 e^{-\ell/a}, \quad \alpha = \frac{a}{\xi}. \tag{13}$$

This relation between the conductance and the link size implies a probability distribution of conductances that decays faster than any power law:

$$P(\Gamma) \sim \frac{1}{\Gamma}e^{-\alpha^d\left(\ln\left(\frac{\Gamma_0}{\Gamma}\right)\right)^d} \qquad \text{for} \quad \Gamma \gg \epsilon\frac{\kappa_0}{a^{2-d}}. \tag{14}$$

This contrasts with the power-law distribution obtained in one dimension $P(\Gamma) \sim (\Gamma_0/\Gamma)^{1-\alpha}$.

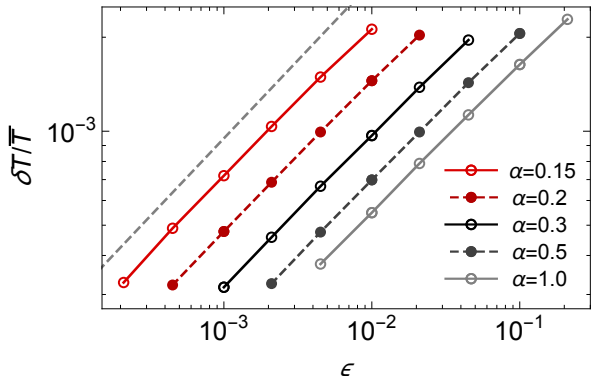


FIG. 4. Fluctuations of the local temperatures, $\delta T/\bar{T}$ as function of the coupling strength ϵ to non-thermal baths, computed from a two-dimensional resistor network model with conductances (13) distributed as in Eq. (14). For $\epsilon \to 0$, a diffusive behavior with temperature fluctuations described by $\delta T/\bar{T} \sim \epsilon^{d/2z}$ with $z = 2$ is observed for all α. The gray dashed line shows $\delta T/\bar{T} \sim \epsilon^{1/2}$ for comparison. Parameters: $\kappa_0 = 1$, $a\Gamma_0 = 5.0$, $T_0 = 1$, $\delta g_1 = 0.05$, $\delta g_2 = 0.05$, $\theta = T_0$ $N \times N$ system with $N = 100$. Averaging over 500 configurations is performed.

Fig. 4 shows temperature fluctuations as a function of coupling strength to the environment ϵ for $d = 2$. For all values of ξ we see a dependence $\delta\beta/\bar{\beta} \sim \epsilon^{1/2}$ consistent with diffusive behavior $z = 2$. This is in contrast to one dimension where we observed a continuously varying dynamical exponent $z \sim \xi/a$. This observation confirms the expectation [43] that Griffiths effect are absent in $d > 1$ where insulating regions cannot serve as bottlenecks, but are rather short-circuited by surrounding smaller resistivities.

Current dependence on the dynamical exponent

As an alternative to temperature fluctuations, we proposed in the main text, a setup that is driven via a small bias at the edges. In the bulk, the system is still coupled to phonons but not necessarily driven. The information about the dynamical exponent is in this case contained in

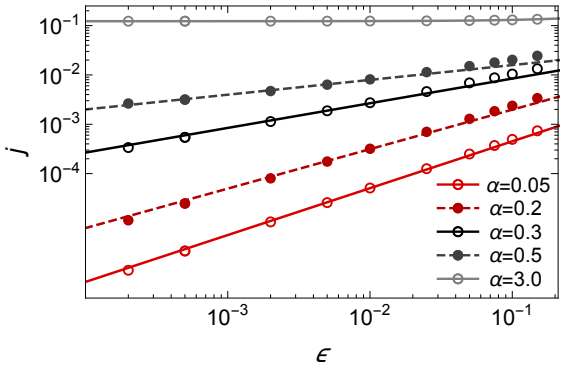


FIG. 5. Dependence of particle current j on the strength of coupling to the baths ϵ in $d = 1$. For $\alpha < 1$, $j \sim \epsilon^{1-\alpha}$ is observed. For diffusive $\alpha > 1$, on the other hand, a finite $j(\epsilon \to 0)$ is observed. Parameters: $\sigma_0 = 1$, $a\tilde{\Gamma}_0 = 5.0$, $N = 2000$, $V = 0.1N$

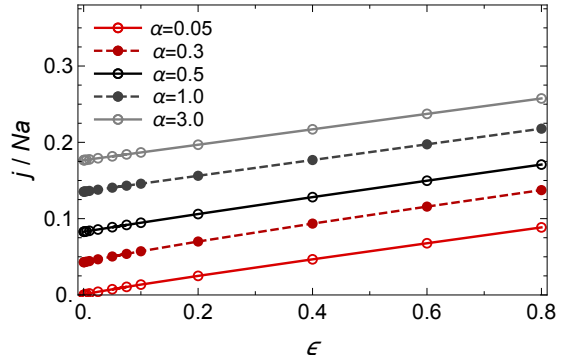


FIG. 6. In $d = 2$ dimension, current density j/Na shows a similar behavior as the $d = 1$ diffusive case ($\alpha > 1$) and can be, to a good approximation, fitted with $c_1 + \epsilon c_2$. Parameters: $a\tilde{\Gamma}_0 = 5$, $\sigma_0 = 1$, system of $N \times N$ sites for $N = 100$, $V = 0.1N$.

the dependence of the current on the strength of coupling to the thermal phonon bath. The average resistivity, obtained by taking an ensemble average of the local conductances, was $\bar{\rho} \sim \left(\epsilon / \ln \epsilon^{-1}\right)^{\alpha-1}$, where $\alpha = a/\xi \sim 1/z$.

In this section we compute the resistance of the network in one and two dimensions, obtained through numerical solution of the steady state rate equations. In the one dimensional case, for example, Kirchoff's law is

$$\left(\tilde{\Gamma}_{i,i+1}(\mu_{i+1} - \mu_i) - \tilde{\Gamma}_{i-1,i}(\mu_i - \mu_{i-1})\right) = 0. \qquad (15)$$

In this case we set up a voltage bias across the chain $V = \mu_0 - \mu_N$, then solve for the island chemical potentials μ_i to get the current. As in the thermal case, we draw the link sizes along the chain from the distribution $p(\ell) \sim e^{-(\ell/\xi)^d}$, while the link conductances are:

$$\tilde{\Gamma} = \epsilon \frac{\sigma_0}{\ell^{2-d}} + \tilde{\Gamma}_0 e^{-\ell/a} \qquad (16)$$

In the two dimensional case we set up a constant chemical potential $\mu = V$ on the left edge and a constant $\mu = 0$ on the right edge.

The result of the calculation of the current in a one dimensional chain for the case $\alpha < 1$ is shown in Fig. 5. The result agrees well with the analytic prediction for the resistance scaling as $\epsilon^{\alpha-1}$, which was obtained in the main text up to logarithmic corrections. In the diffusive regime ($\alpha > 1$), the current has a non-zero $\epsilon \to 0$ limit, as we expect for a system with finite intrinsic resistivity. Also in two dimension we always find a finite resistivity in the $\epsilon \to 0$ as well as linear corrections, as shown in Fig. 6.

Remember that the dynamical exponent is related to α as $z \sim \alpha^{-1}$. Measuring the dependence $j(\epsilon, \alpha)$ in a disordered system would therefore provide information on z and it's divergence upon approaching the MBL transition even in disordered materials that are weakly coupling to phonons. The strength of coupling to phonons ϵ can be tuned by controlling the phonon temperature; see our previous work [18], where we showed that phonon temperature determines the effective coupling.

Comparison to standard measures of dynamical scaling

In this section we verify that the dynamical exponent z obtained from the temperature variations, through the relation $\delta T \sim \epsilon^{d/2z}$ is identical to the standard measure of dynamical scaling obtained from spreading of an energy fluctuation. To obtain the standard measure of z we consider an initially localized energy profile in the random resistor network $e_i = \delta_{i,x_0}$. We determine z by measuring the width of the energy packet $\sigma_E = \sqrt{\sum_i (i - x_0)^2 \tilde{e}_i(t)}$ and fitting it to a power law

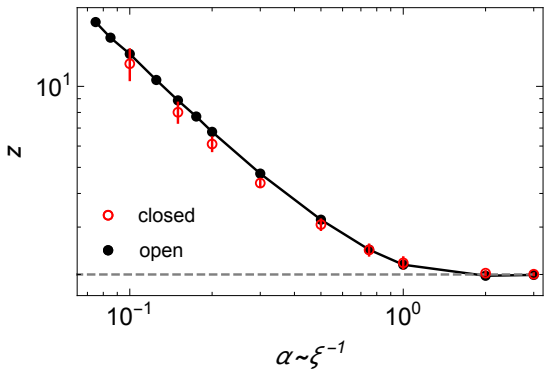


FIG. 7. Comparison of the dynamical exponent z calculated from the fluctuations of the local temperatures (open) or from the from anomalous heat diffusion in a closed system (closed). Parameters: $\kappa_0 = 1$, $a\Gamma_0 = 5.0$, $T_0 = 1$, $\delta g_1 = 0.05$, $\delta g_2 = 0.05$, $\theta = T_0$, $N = 1000$, averaged over $M = 500$ configurations.

$\sigma_E \sim t^{1/z}$. Here $\tilde{e}_i(t) = \langle\langle e_i(t)\rangle\rangle$ is a disorder averaged energy distribution. For each realization of the disorder $e_i(t)$ is calculated using the continuity equation with $\epsilon = 0$:

$$\partial_t e_i - \Gamma_{i,i+1}(T_{i+1} - T_i) + \Gamma_{i-1,i}(T_i - T_{i-1}) = 0 \quad (17)$$

Note that here $\Gamma = \Gamma_0 e^{-\ell/a}$. Fig. 7 shows a qualitative agreement between the value of z obtained via these two different approaches.

Convergence in system size, time and bond dimension

In this section, we look more closely into what are the limiting factors of the calculation. We first investigate how our results on system size $N = 20$ depend on the bond dimension. Fig. 8 shows the relative change of the expectation value of $O = \delta\beta/\beta(\epsilon)$ with bond dimension χ at steady state. We set $\chi = 100$, used for the results in the main text, as a baseline. $O(\chi)$ is averaged over 60 disorder realizations, which are the same for different χ. We find that the error extrapolated to $\chi = \infty$ is small, e.g., for $h = 4$ below 0.1%. We also note that the extrapolated error estimate grows with decreasing ϵ, hence for smaller values of ϵ a larger bond dimension will be required, increasing the costs of computations at small ϵ.

In Fig. 9 we show the relaxation of temperature fluctuations $O(t) = \frac{\delta\beta}{\beta}(t)$ to steady state in the TEBD time evolution. Specifically, we plot $|O(t) - O(t_f)|$ with respect to the $O(t_f)$ at the maximal propagation time t_f. As expected, we see exponential relaxation to the steady-state value with a characteristic rate which scales as ϵ. Obtaining results for smaller ϵ is thus increasingly hard with TEBD.

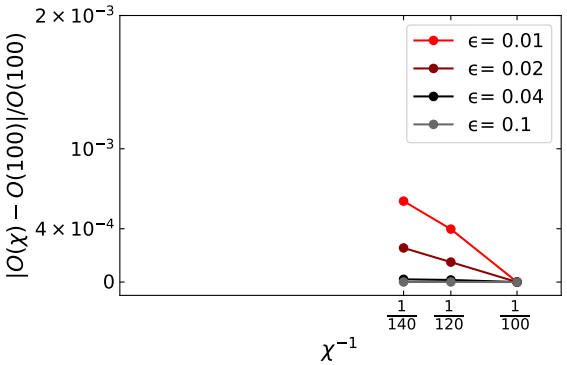


FIG. 8. Relative error due to finite bond dimension $\chi = 100$ can be estimated from the ratio $|O(\chi) - O(\chi = 100)|/O(\chi = 100)$, $O(\chi) = \frac{\delta\beta}{\beta}(\chi)$. The error estimated from the $\chi \to \infty$ extrapolation is below 0.1% for smallest $\epsilon = 0.01$ used in our computations. Parameters: $N = 20$, $h = 4$, with averaging over 60 realizations.

Assuming that the necessary bond dimension χ is independent of system size, our approach should be scalable, with computational demands growing linearly with system size. Figs. 9(a,b) compare the convergence of $O(t) = \frac{\delta\beta}{\beta}(t)$ for a single realization at $N = 20, 40$ system sizes. While the computational time approximately doubles, the exponential convergence rate with TEBD evolution time t is comparable.

Finally, we present a finite size scaling analysis of the results. We show the dependence of the dynamical exponent z, obtained from our numerical scheme, on the system size. The exponent z is extracted by fitting a power law for the dependence of the temperature variance on ϵ with $\epsilon \geq 0.01$, Eq.(9) in the main text. The results are shown in Fig. 10.

In systems with disorder strengths $h = 2.0, 3.0, 4.0$ we do observe negligible finite size dependence. Recall that this is the range of h we used to extract the power law divergence of $z \sim (h_c - h)^{-\nu}$ on approaching the critical point. It is encouraging to see that this behavior is unaffected by finite size. We do see a non systematic finite size dependence for disorder strength $h = 4.5$, which we attribute to uncertainty in fitting the dynamical exponent z. Indeed, as noted in the main text, for $h > 4$

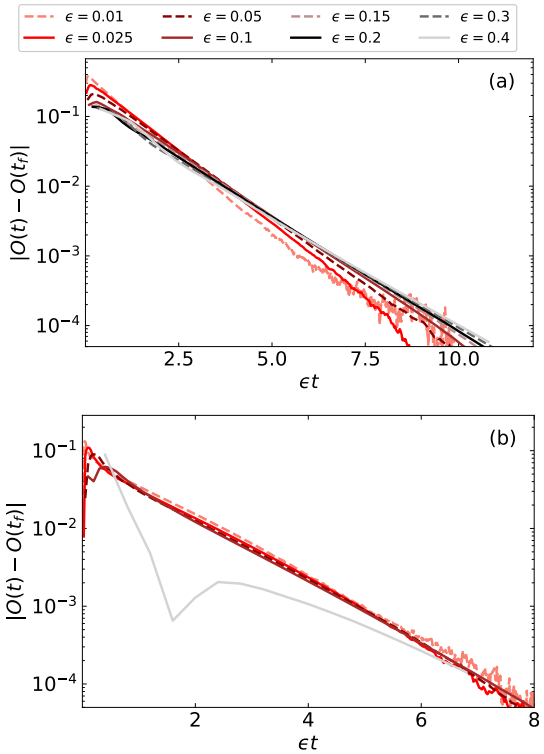


FIG. 9. Evolution of $O(t) = \frac{\delta\beta}{\beta}(t)$ (with respect to $O(t_f)$ at maximal propagation time t_f) during the TEBD computation, for one disorder realization at $h = 4$, $\chi = 100$, for systems of size (a) $N = 20$ and (b) $N = 40$. Note that the time axis is rescaled by ϵ to reveal an exponential relaxation with a convergence rate proportional to ϵ.

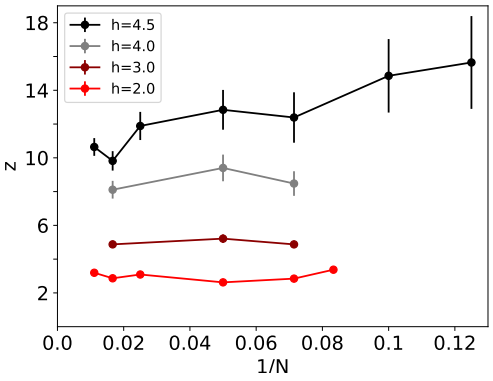


FIG. 10. Finite-size analysis of the dynamical exponent z for $h = 2.0, 3.0, 4.0, 4.5$. Calculations are performed with bond dimension $\chi = 100$ and $\epsilon \geq 0.01$. A different number of realizations is used for different points, e.g., at $h = 2.0$ and $N \in [12, 90]$, $150 - 50$ realizations are used, for $h = 4.5$ and $N \in [8, 90]$, $790 - 190$ realizations are used. Fit error bars are obtained with the jackknife resampling of data with $\epsilon \geq 0.01$ and do not estimate systematic deviations from the z that would be obtained using $\epsilon < 0.01$, necessary for $h > 4$.

($z > 8$) we can no longer extract a reliable power law fit to $\frac{\delta\beta}{\beta} \sim \epsilon^{\frac{1}{2z}}$ in the range $\epsilon \geq 0.01$. In order to reliably obtain larger values of z close to the critical point one would have to reduce the cutoff ϵ exponentially in z (equivalently, in ξ). Thus it is the finite time cutoff $(1/\epsilon)$ rather than the finite size, which limits the calculation.

As noted in the main text, calculations performed at smaller ϵ might yield somewhat larger h_c as well, which would, in turn, impact the value of ν obtained from $z \sim (h_c - h)^{-\nu}$ fit.

Hydrodynamic equations as an expansion of Lindblad driving

In the main text we introduced the hydrodynamic approach as an effective description of a system that is coupled to a thermal (e.g. phonon) bath and to a drive (e.g. white light). Here we make the connection to the microscopic calculation, that was performed for a spin chain coupled to Markovian nonequilibrium baths described by Lindblad operators. We show that the hydrodynamic Eq. (1) can be derived using an expansion in small temperature variations around the thermal density matrix, determined from the Liouville equation $\dot{\rho} = (\hat{\mathcal{L}}_0 + \epsilon\hat{\mathcal{D}})\rho = 0$, where $\hat{\mathcal{L}}_0\rho = -i[H, \rho]$ and $\hat{\mathcal{D}}$ corresponds to the dissipator super-operator.

On the ergodic side, the system approaches a thermal state for $\epsilon \to 0$ [18]. For small epsilon, we can therefore expand the steady state density matrix in weak temperature variations around the thermal state

$$\rho \approx \rho_0(\bar{T}) + \sum_j \delta T_j \frac{\partial\rho}{\partial T_j}\Big|_{T_j=\bar{T}} + \cdots, \quad \rho_0(\bar{T}) \equiv \frac{e^{-H/\bar{T}}}{\mathrm{Tr}[e^{-H/\bar{T}}]} \tag{18}$$

We will now use the expansion (18) in order to show how the phenomenological terms in Eq. (1) can emerge from the microscopic Liouville equation.

First of all, the term $-\epsilon\bar{g}(T(\boldsymbol{r}) - \bar{T}))$ ensures the relaxation towards the correct mean temperature $\bar{T}$, which is determined from the stationarity condition applied to the total rate equation for the energy [18],

$$\langle\dot{H}\rangle = \mathrm{Tr}[H(\hat{\mathcal{L}}_0 + \epsilon\hat{\mathcal{D}})\rho_0(\bar{\beta})] = \mathrm{Tr}[H\,\epsilon\hat{\mathcal{D}}\,\rho_0(\bar{\beta})] \stackrel{!}{=} 0 \tag{19}$$

To see the emergence of the other terms in Eq. (1) we consider the behaviour of the local energy density $\langle h_i\rangle$, where $H = \sum_i h_i$,

$$\frac{d}{dt}\langle h_i\rangle = \mathrm{Tr}\left[h_i\hat{\mathcal{L}}_0\rho\right] \tag{20}$$

$$+ \mathrm{Tr}\left[h_i\epsilon\hat{\mathcal{D}}\rho_0(\bar{\beta})\right] \tag{21}$$

$$+ \mathrm{Tr}\left[h_i\epsilon\hat{\mathcal{D}}\sum_j \frac{\partial\rho}{\partial T_j}\Big|_{T_j=\bar{T}}\delta T_j\right] \tag{22}$$

$$+ \cdots$$

Using the definition for the energy currents, $j_{i,i+1} = i[h_i, h_{i+1}]$, we can see that the right hand side of expression (20) equals to the difference in expectation value of energy currents across neighboring links. On the other hand, in a system with spatially varying local temperatures, local current expectation values are proportional to local temperature gradients

$$\mathrm{Tr}\left[h_i\hat{\mathcal{L}}_0\rho\right] = \mathrm{Tr}[(-j_{i,i+1} + j_{i-1,i})\rho] \tag{23}$$

$$= \Gamma_{i,i+1}(T_{i+1} - T_i) - \Gamma_{i-1,i}(T_i - T_{i-1})$$

$$\sim \nabla\cdot(\kappa(\boldsymbol{r})\nabla T(\boldsymbol{r})) \tag{24}$$

The term (21) corresponds to the gain and loss of local energy density due to the driving and dissipation, evaluated with respect to the homogeneous thermal state

$$\mathrm{Tr}\left[h_i\epsilon\hat{\mathcal{D}}\rho_0(\bar{\beta})\right] \sim \epsilon\,\theta g_2(\boldsymbol{r}). \tag{25}$$

Here $\langle g_2(\boldsymbol{r}_i)\rangle = \frac{1}{\theta N}\sum_i \mathrm{Tr}[h_i\hat{\mathcal{D}}\rho_0(\bar{\beta})] = 0$ due to Eq. (19).

Term (22) is of the same type, but comes from the next order expansion in the variation of local temperatures

$$\mathrm{Tr}\left[h_i\epsilon\hat{\mathcal{D}}\sum_j \frac{\partial\rho}{\partial T_j}\Big|_{T_j=\bar{T}}\delta T_j\right] \sim \epsilon g_1(\boldsymbol{r})\,\delta T(\boldsymbol{r}) \tag{26}$$

Collecting the dominant terms in the $(\delta T(\boldsymbol{r}))^n$ expansion, we get the hydrodynamic relation

$$\partial_t e - \nabla\cdot(\kappa(\boldsymbol{r})\,\nabla T(\boldsymbol{r})) = -\epsilon\, g_1(\boldsymbol{r})(T(\boldsymbol{r}) - \bar{T}) + \epsilon\,\theta g_2(\boldsymbol{r}) \tag{27}$$

which can be identified with Eq. (1), except that T_0 is replaced by $\bar{T}$ (set by Eq. 19) and that the last term contains only the random part with a zero mean, i.e., $g_2(\boldsymbol{r}) = \delta g_2(\boldsymbol{r})$.